Biochemical Pharmacology 83 (2012) 149–163

Contents lists available at SciVerse ScienceDirect

Biochemical Pharmacology

journal homepage: www.elsevier.com/locate/biochempharm

Comparison of the function and expression of CYP26A1 and CYP26B1, the two retinoic acid hydroxylases

Ariel R. Topletz [a,1], Jayne E. Thatcher [a,1], Alex Zelter [b], Justin D. Lutz [a], Suzanne Tay [a], Wendel L. Nelson [c], Nina Isoherranen [a,*]

[a] Department of Pharmaceutics, University of Washington, Seattle, WA, United States
[b] Department of Biochemistry, University of Washington, Seattle, WA, United States
[c] Department of Medicinal Chemistry, University of Washington, Seattle, WA, United States

ARTICLE INFO

Article history:
Received 9 September 2011
Accepted 7 October 2011
Available online 14 October 2011

Keywords:
Vitamin A
Cytochrome P450
Retinoic acid
Metabolism
Tissue expression

ABSTRACT

All-trans-retinoic acid (*at*RA) is an important signaling molecule in all chordates. The cytochrome P450 enzymes CYP26 are believed to partially regulate cellular concentrations of *at*RA via oxidative metabolism and hence affect retinoid homeostasis and signaling. CYP26A1 and CYP26B1 are *at*RA hydroxylases that catalyze formation of similar metabolites in cell systems. However, they have only 40% sequence similarity suggesting differences between the two enzymes. The aim of this study was to determine whether CYP26A1 and CYP26B1 have similar catalytic activity, form different metabolites from *at*RA and are expressed in different tissues in adults. The mRNA expression of CYP26A1 and CYP26B1 correlated between human tissues except for human cerebellum in which CYP26B1 was the predominant CYP26 and liver in which CYP26A1 dominated. Quantification of CYP26A1 and CYP26B1 protein in human tissues was in agreement with the mRNA expression and showed correlation between the two isoforms. Qualitatively, recombinant CYP26A1 and CYP26B1 formed the same primary and sequential metabolites from *at*RA. Quantitatively, CYP26B1 had a lower K_m (19 nM) and V_{max} (0.8 pmol/min/pmol) than CYP26A1 (K_m = 50 nM and V_{max} = 10 pmol/min/pmol) for formation of 4-OH-RA. The major *at*RA metabolites 4-OH-RA, 18-OH-RA and 4-oxo-RA were all substrates of CYP26A1 and CYP26B1, and CYP26A1 had a 2–10-fold higher catalytic activity towards all substrates tested. This study shows that CYP26A1 and CYP26B1 are qualitatively similar RA hydroxylases with overlapping expression profiles. CYP26A1 has higher catalytic activity than CYP26B1 and seems to be responsible for metabolism of *at*RA in tissues that function as a barrier for *at*RA exposure.

1. Introduction

Retinoic acid (RA), the active metabolite of vitamin A, is a critical signaling molecule in animals. RA exists as at least four different isomers: *all-trans*-RA (*at*RA), 9-*cis*-RA, 13-*cis*-RA, and 9,13-*dicis*-RA. Of these, *at*RA is considered to be the biologically active isomer, but 9-*cis*-RA and 13-*cis*-RA also have activity and are marketed as drugs [1]. *at*RA acts by binding to retinoic acid receptors (RARs) regulating gene transcription, thereby having effects on cell cycle and cell survival [1–3]. The observed effects of *at*RA are dependent on its concentrations in the cell as well as on expression levels of RAR isoforms. During development, deficiency or overexposure to RA has detrimental effects resulting in fetal malformations [4,5]. In children and adults, RA signaling is associated with maintenance of immunity and of the epithelia, reproduction and spermatogenesis, regulation of glucose homeostasis, cell cycle and apoptosis, and maintenance of neurogenesis and neuronal cell survival [1,6–8].

Dietary intake of *at*RA precursors, synthesis of *at*RA from retinol and retinal, and the metabolism of *at*RA collectively determine the concentration of *at*RA in specific tissues and cells. The CYP26 enzymes appear to be responsible for metabolism of *at*RA in all chordates and hence are believed to contribute to regulation of *at*RA homeostasis and signaling [9–11]. The CYP26 family consists of three isoforms: CYP26A1, CYP26B1 and CYP26C1, which fulfill different function but their specific roles are not well understood [9]. Recombinant CYP26A1 forms three primary hydroxylated products, 4-OH-RA, 18-OH-RA and 16-OH-RA, and a number of sequential metabolites from *at*RA [12–14]. Based on studies in transfected cell lines, both CYP26A1 and CYP26B1 are hydroxylases that form 4-OH-RA and 18-OH-RA from *at*RA [14–16], whereas CYP26C1 appears to

* Corresponding author at: Department of Pharmaceutics, University of Washington, Box 357610, Seattle, WA 98195-7610, United States.
Tel.: +1 206 543 2517; fax: +1 206 543 3204.
E-mail address: ni2@u.washington.edu (N. Isoherranen).
[1] These two authors contributed equally to this work.

0006-2952/$ – see front matter © 2011 Elsevier Inc. All rights reserved.
doi:10.1016/j.bcp.2011.10.007

prefer 9-*cis*-RA as a substrate [16]. The similar proposed catalytic characteristics of these isozymes are of interest because the amino acid sequence identity between the CYP26 proteins is only 42–51% [15,16], suggesting that there are structural differences between these proteins. However, no studies comparing the catalytic activities or the metabolites formed by recombinant CYP26A1 and CYP26B1 have been published. Since many oxidative metabolites, such as 4-OH-RA, 4-oxo-RA and 18-OH-RA, formed from *at*RA by P450s have pharmacological activity and bind to RARs [17], it is possible that different metabolites formed by the CYP26 isoforms contribute to their *in vivo* functional differences.

During mouse development, the expression of the CYP26 isoforms is distinct in a spatio-temporal manner [18,19]. In human fetal tissues CYP26A1 seems to be expressed exclusively in the brain whereas CYP26B1 was not present in the brain but found in all other tissues tested. *Cyp26a1*$^{-/-}$ and *Cyp26b1*$^{-/-}$ mice have distinct phenotypes and CYP26A1 and CYP26B1, but not CYP26C1, are essential for healthy development [19–22]. The requirement of CYP26A1 and CYP26B1 for healthy development is likely due to specific expression patterns and different regulation. Whether the same applies to adult tissues is not known and the expression pattern of CYP26A1 and CYP26B1 in adult tissues is not well characterized. mRNA and protein data suggest that CYP26A1 expression is high in the liver whereas CYP26B1 mRNA is low or undetected in human liver [23–25]. Based on single donor mRNA, CYP26B1 has ubiquitous expression in adult human tissues [15]. Despite the detection of mRNA, no data on corresponding protein expression are available. However, *at*RA metabolism has been shown in rat testes, kidney, liver and lung microsomes [26], although the metabolite ratios were different between tissues suggesting different CYPs contribute to the metabolism in different tissues. Based on these data, it was hypothesized that CYP26A1 and CYP26B1 have different catalytic characteristics and different tissue distribution in adult tissues.

To test whether CYP26A1 and CYP26B1 are functionally similar *in vitro* and have distinct tissue expression patterns, CYP26A1 and CYP26B1 mRNA and protein expression were characterized in selected human tissues, CYP26A1 and CYP26B1 were expressed using baculovirus infected insect cells, the kinetics of formation of 4-OH-RA and 18-OH-RA were examined, and the elimination of 4-OH-RA, 4-oxo-RA and 18-OH-RA by CYP26A1 and CYP26B1 were determined. In addition, the sequential metabolites formed from *at*RA by the two CYPs were identified. The results provide the first characterization of recombinant CYP26B1 and the first comparison of the function and expression patterns of CYP26A1 and CYP26B1.

2. Materials and methods

2.1. Chemicals and enzymes

*at*RA, acitretin, cholic acid, imidazole and NADPH were purchased from Sigma–Aldrich (St. Louis, MO). 4-OH-RA and 4-oxo-RA (Fig. 1) were synthesized as previously described [13,27]. Rat P450 reductase was expressed in *Escherichia coli* and purified as previously reported [28]. CYP26A1 was expressed in Sf9 cells and microsomes were prepared as previously described [13]. All Supersomes® were co-expressed with reductase and, with the exception of CYP4A11, CYP1A1, CYP1A2, CYP2C18 and CYP2D6, with cytochrome b5 and purchased from BD Gentest (BD Biosciences, Woburn, MA). Nonidet P40, phenymethanesulfonyl fluoride (PMSF) and complete EDTA-free protease inhibitor cocktail tablets were purchased from Roche (Indianapolis, IN). Potassium chloride was purchased from Fisher Scientific (Pittsburgh, PA). Sodium phosphate and glycerol were obtained from JT

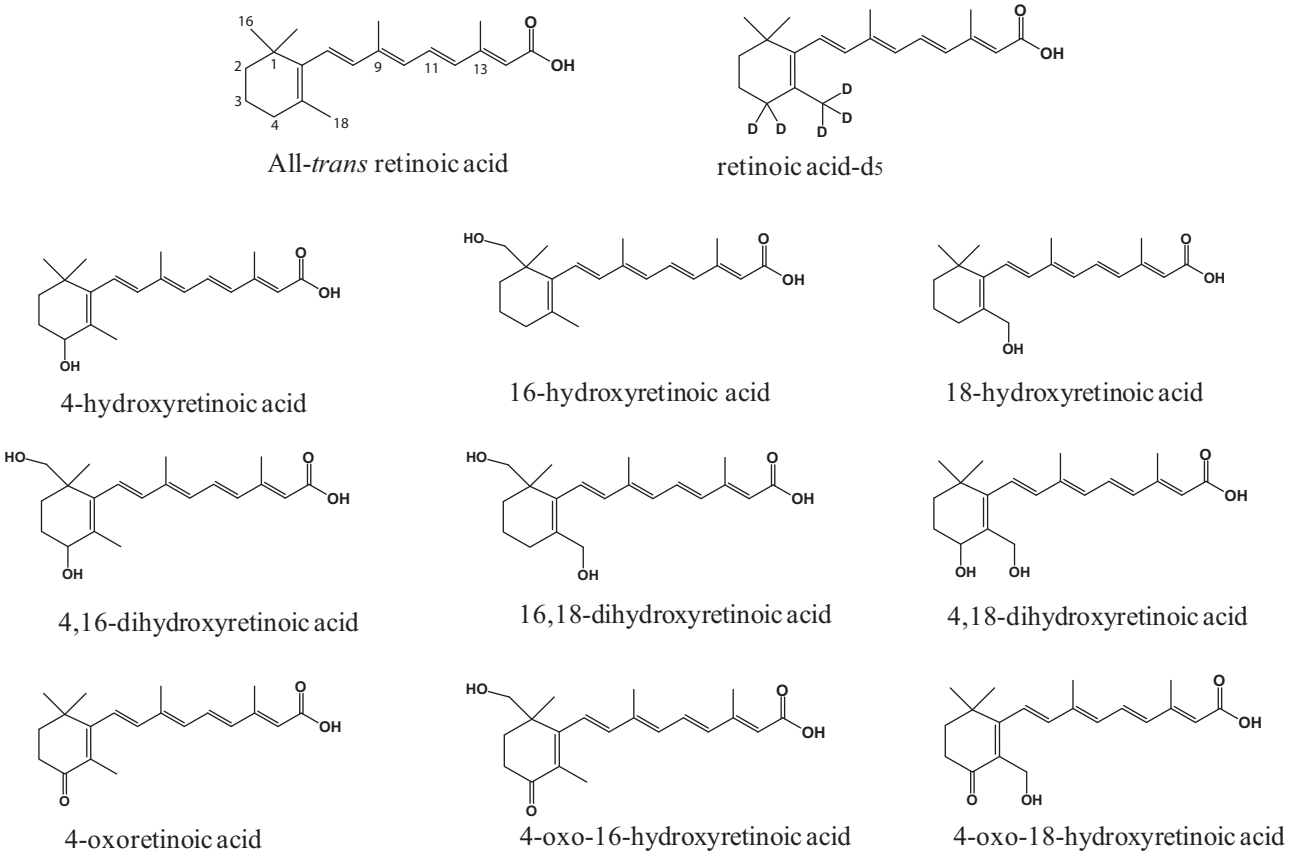

Fig. 1. Chemical structures of *at*RA, *at*RA-d_5, and detected or proposed *at*RA metabolites.

Baker (Phillipsburg, NJ). All solvents used for HPLC–UV and chemical synthesis were HPLC grade or higher and were purchased from EMD Chemicals (Gibbstown, NJ), JT Baker (Phillipsburg, NJ), or Fisher Scientific (Pittsburgh, PA). All solvents and water used for LC–MS studies were Optima grade obtained from Fisher Scientific (Pittsburgh, PA).

2.2. Synthesis of 18-OH-RA

The 18-OH-RA (Fig. 1) was synthesized from 2-formyl-6,6-dimethylcyclohexanone as previously described [29,30] with two important modifications. The isomerization of the mixture of 11-*cis*- and 11-*trans*-isomers of the intermediate 18-acetate ester of ethyl retinoate to the 11-all-*trans* diester was effectively accomplished using palladium nitrate, a more easily removed water soluble catalyst [31], and the final product was obtained by alkaline hydrolysis of both the 18-acetate and 15-ethyl esters under mild conditions, a one-step procedure that avoids the multi-step exchange of protecting groups reported previously [29,30].

2.2.1. Palladium nitrate catalyzed isomerization

To a solution of 18-OH-retinoic acid diester (18-acetate, 15-ethyl ester) (91 mg, 0.24 mmol) in acetonitrile (1 mL) 50 °C, 18.2 μL from a solution of palladium nitrate (5.0 mg, 22 μmol) and triethylamine (4.8 mg, 47 μmol) in acetonitrile (1 mL) was added (retinoid to palladium catalyst ratio of 1:1000, w/w). The reaction mixture was kept at 50 °C overnight, and the conversion from the 11-*cis*- to all-*trans*-isomer was monitored by HPLC–UV. HPLC–UV analysis was performed using an Agilent Technologies (Palo Alto, CA) 1200 series HPLC system with an Agilent Technologies Extend C18 3.5 μm column (2.1 mm i.d. × 100 mm). mm). The analytes were separated over a 28 min gradient elution using mobile phases of aqueous 50 mM ammonium acetate buffer (pH 4.5) and acetonitrile. The initial conditions were 90:10 buffer:acetonitrile. Acetonitrile was increased linearly over 15 min to reach a final condition of 10:90 buffer:acetonitrile, which was then held for another 13 min before returning to the initial conditions. Analytes were detected using a multiple wavelength UV detector, monitoring wavelengths at 342 nm and 360 nm. Data analysis was performed using HP Chemstation software. Retention times for the 18-acetoxy regioisomers of the all-*trans*-, 11-*cis*- and 9-*cis*-retinoic acid esters were 24.9 min, 25.3 min, and 25.6 min, respectively.

At completion, the organic solvents were evaporated and the residue dissolved in 10 mL of methylene chloride. Palladium nitrate was extracted with 2 × 5 mL water, and the organic phase was dried over sodium sulfate, filtered and evaporated to dryness. Yield: 92% (84 mg, 0.22 mmol).

2.2.2. Hydrolysis to 18-hydroxyretinoic acid

To a solution of the all-*trans*-18-OH-retinoic acid diester (18-acetate, 15-ethyl ester) (84 mg, 0.22 mmol) in methanol (5 mL) at 0 °C (ice bath) was added 5 mL of a 2 M KOH solution in methanol:water (1:9), also at 0 °C. Hydrolysis was monitored by TLC (1% acetic acid, ethyl acetate/hexanes, 25:75); RF = 0.75 (diester) and RF = 0.10 (product). After 5 h, an additional 3 mL of the 2 M KOH solution was added and the mixture was stirred for an additional 8.5 h at room temperature. The reaction mixture was adjusted to pH 6 using 1 M pH 6 citrate buffer and 1 M citric acid at −10 °C (ice $CaCl_2$ bath). The 18-OH-RA was extracted with ethyl acetate (2 × 100 mL). After NaCl was added to the remaining aqueous layer, the mixture was extracted with additional ethyl acetate (2 × 100 mL). The combined organic extracts were washed with brine, dried over sodium sulfate, and evaporated to dryness. 18-OH-RA was isolated by HPLC–UV, using conditions as previously described [25] (retention time of 18-OH-RA = 16.8 min). ^{1}H NMR ($CDCl_3$, 500 MHz): δ 6.96 (dd, 1, J = 15, 12 Hz, H-11), 6.26 (d, 1, J = 15 Hz, H-12), 6.12 (d, 1, J = 11.5 Hz, H-10), 6.20 (d, 1, J = 16 Hz, H-8), 6.10 (d, 1, J = 16 Hz, H-7), 5.75 (s, 1, H-14), 4.07 (s, 2, 18-CH_2O), 2.30 (s, 3, 20-CH_3), 2.15 (m, 2, 4-CH_2), 1.94 (s, 3, 19-CH_3), 1.60 (m, 2, 3-CH_2), 1.44 (m, 2, 2-CH_2), 0.97 (s, 6, 16,17-CH_3). Accurate mass of the synthetic product was obtained using a Waters ACQUITY UPLC and autosampler coupled to a Waters Micromass Synapt Ion Mobility Q/TOF hybrid MS/MS mass spectrometer operated in negative electrospray mode (Milford, MA). Ten microliters of a 100 nM sample in 50:50 acetonitrile:water was injected into a 50:50 acetonitrile:water isocratic flow (50 μL/min). The detection settings used were as follows: a capillary voltage of −3.3 kV, a trap collision energy of −6.0 V and a transfer collision energy of −4.0 V. An MS spectra was obtained over a range of 50–1000 m/z. Leucine enkephalin (M−1 = 554.2615 m/z) was infused at 5 μL/min and utilized as an internal calibrant (lock mass) at an interval of 1 scan every 10 s. The accurate mass of the product was 315.1966 m/z (calc 315.1960 m/z, 1.9 ppm accuracy).

2.3. Human tissue mRNA and quantitative real-time PCR

Single donor tissue total RNA was obtained from Biochain (Hayward, CA). Skin total RNA was a gift from Dr. Ed Kelly (University of Washington, Seattle, WA) and was also obtained from Biochain but was a pooled sample of 5 donors. mRNA was quantified and RNA quality confirmed as previously described [23]. Taqman real-time Universal PCR Master Mix and PCR primers and fluorescent probes were obtained from Applied Biosystems (Foster City, CA). Probes were labeled with the 5′ reporter dye FAM but without a quencher on the 3′ end. Primer and probe pairs used included: CYP26A1 (Hs00175627_m1), CYP26B1 (Hs00219866_m1) and GAPDH (Hs99999905_m1). Complimentary DNA (cDNA) was generated by reverse transcription using the Taqman reverse transcription reagents kit (Applied Biosystems, Foster City, CA) and 1 μg total RNA according to manufacturers recommendations. Quantitative real-time PCR was conducted on a StepOnePlus Real-Time PCR instrument (Applied Biosystems, Foster City, CA) using 1 holding stage cycle of 50 °C for 2 min, then 95 °C for 10 min and 40 cycles of 95 °C for 15 s and 60 °C for 1 min. Real-time analysis was done in duplicate for each sample and the average between the two was used in calculations. The expression of CYP26A1 and CYP26B1 was quantified as absolute mRNA expression as described previously using linearized CYP26A1 and CYP26B1 plasmid as a standard curve [23]. GAPDH mRNA was quantified as a quality control.

2.4. Cloning and expression of CYP26B1

CYP26B1 cDNA was obtained from OriGene Technologies (Rockville, MD) (catalog number TC120799). Primers were designed (forward primer sequence: 5′-gcgaattcat gctctttgag ggcttgg-3′; reverse primer sequence: 5′-gcaagctttt aatggtgatg gtgatgatgt ccctgaaaat acaggttttc gactgtggcg ctcagcatggc-3′) to amplify the CYP26B1 coding sequence while adding the following features: (1) an EcoRI site immediately upstream of the open reading frame; (2) a TEV cleavage site and 6xHis tag prior to the stop codon; and (3) a HindIII site immediately after the stop codon. The resulting PCR product was cloned into the Invitrogen Zero Blunt TOPO vector according to the manufacturer's instructions. EcoRI and HindIII were used to excise the His-tagged CYP26B1 gene from the TOPO vector and the resulting fragment was ligated into pFastBac (Invitrogen). The Bac-to-Bac baculovirus expression system (Invitrogen) was used to produce protein from Sf9 cells according to the manufacturer's instructions using Sf-900 II SFM liquid media (Invitrogen) supplemented with 2.5% fetal bovine serum. During protein expression ferric citrate (0.2 mM) and δ-aminolevulinic acid (0.3 mM) were added to the media 24 h post-infection to facilitate

heme synthesis. The cells were harvested 48 h post-infection, washed once in PBS with 1 mM PMSF, pelleted and stored at −80 °C.

2.5. Preparation of membrane fractions from insect cells

Cell pellets were thawed in a 37 °C water bath and then kept on ice. Ice-cold homogenizing buffer (10 mM KPi, pH 7.4, 10 mM EDTA, 0.15 M KCl, 1 mM DTT, 0.1 mM PMSF and a protease inhibitor cocktail) was added and cells were disrupted and microsomes prepared using a homogenizing tube and a Teflon pestle. To isolate membrane fraction, the homogenates were centrifuged at 100,000 × *g* for 90 min at 4 °C, and the pellet was resuspended in storage buffer (50 mM KPi, pH 7.4, 20% glycerol, and 1 mM EDTA). The P450 content of the membrane preparations was determined by a CO difference spectrum [32] using a Cary UV–vis spectrophotometer (Varian, Palo Alto, CA). Protein concentrations of the membrane preparations were measured using a Pierce (Rockford, IL) BCA protein assay reagents according to the manufacturer's instructions.

2.6. Purification of CYP26B1

For purification of CYP26B1, a frozen cell pellet was resuspended in solubilization buffer (50 mM KPi containing: 20% glycerol, 1% NP40, 1% cholate, and protease inhibitor cocktail). The protein solution was sonicated and centrifuged at 50,000 × *g* for 30 min. The soluble fraction (supernatant) was applied to a talon (cobalt affinity) column (4 mL bed volume) equilibrated with three column volumes of 50 mM KPi buffer with 150 mM KCl, 20% glycerol and 10 mM imidazole. The column was then washed with 15 mL of the solubilization buffer, 30 mL of solubilization buffer with 20 mM imidazole added, and 15 mL of 50 mM KPi with 20% glycerol and 150 mM KCl. The purified CYP26B1 was eluted with 500 mM imidazole in 50 mM KPi buffer with 20% glycerol and 150 mM KCl. Samples were run on a 10% SDS-PAGE gel and stained with Coomassie dye to detect purity and identify fractions containing CYP26B1. Fractions containing CYP26B1 were combined and buffer exchanged to 50 mM KPi, 150 mM KCl and 20% glycerol and concentrated using Amicon Ultra Spin Columns (Millipore, Billerica, MA). The concentration of active P450 in the purified protein solution was determined by a CO difference spectrum.

2.7. Determination of ligand-induced binding spectra

To demonstrate that *at*RA binds to purified CYP26B1 and to characterize the binding mode of *at*RA, ligand-induced binding spectra were recorded using an Aminco DW2 Dual Beam spectrophotometer (Olis Instruments, Bogart, GA), scanning from 500 to 375 nm. Purified CYP26B1 (235 pmol/mL) in 100 mM KPi buffer (pH 7.4) with 20% glycerol was added to the test cuvette and an absolute spectrum of CYP26B1 was obtained. Next, *at*RA was added in increments that corresponded to 12.5 nM concentration increase in the test and reference cuvette, and the absorbance was measured until a saturating concentration of *at*RA was added and the maximum absorption change was achieved. *at*RA was added to both cuvettes to normalize for the absorption of *at*RA at 360–400 nm. The difference spectrum was obtained by subtracting the *at*RA free baseline spectrum from the *at*RA added spectra after normalizing the spectra to 490 nm.

2.8. Validation of a specific antibody against CYP26B1

Two commercial antibodies designed to detect CYP26B1 were purchased from Abnova (Walnut, CA). They included a mouse polyclonal antibody (H00056603-A01) as unpurified serum generated using a peptide of internal CYP26B1 sequence (amino acids 131–231) and a mouse monoclonal antibody (H00056603-M01) also generated against a peptide of amino acids 131–231 in CYP26B1. A third CYP26B1 antibody was prepared in-house as a rabbit polyclonal against a C-terminal peptide of CYP26B1 (peptide sequence DSNQNEILPETEAMLSATV). A cysteine and a KLH conjugate were added to the N-terminus of the peptide. The peptide was synthesized and rabbits were used to generate an anti-hCYP26B1 antibody using standard protocol by Open Biosystems (Thermo Fisher, Huntsville, AL). Rabbits were immunized on day 1 with 500 μg of the CYP26B1 peptide injected to 10 different sites. The antigen (250 μg) was also administered on days 14, 28, and 42. The CYP26B1 antiserum was collected on days 56 and 58, with a total volume of approximately 50 mL collected. The collected antiserum was purified using a Pierce (Thermo Scientific, Rockford IL) AminoLink Immobilization Kit according to the manufacturer's instructions (pH 10 protocol). In brief, the same peptide used to immunize the rabbits was coupled overnight to the provided resin packed column. The remaining active sites were then blocked over the course of 30 min using the provided Quenching Buffer before the column was washed with 1 M NaCl. Antibodies were bound to the column over 1 h and the column was washed with phosphate-buffered saline (PBS). The antibody was eluted with a 0.1 M glycine–HCl (pH 2.5–3) buffer. The purified antibody was then neutralized with 1 M phosphate buffer (pH 9), concentrated using ZebaTM Desalt Spin Columns (Pierce/Thermo Scientific) and 0.05% sodium azide was added to prevent bacterial growth.

The specificity of the CYP26B1 antibodies was tested as previously described for CYP26A1 antibodies [25]. 5 μg CYP26A1 and 10 μg CYP26B1 microsomes, and 20 μg CYP1A1, CYP1A2, CYP2C8, CYP2C9, CYP2C18, CYP2C19, CYP2D6, CYP3A4, CYP3A5, and CYP3A7 Supersomes (BD Biosciences, Woburn, MA) were boiled for 5 min in a buffer containing 2.5% β-mercaptoethanol. The samples were loaded onto 10% polyacrylamide gels and separated using electrophoresis. Proteins were transferred for 1 h with 100 V to a PVDF membrane (Millipore, Billeria, MA). The membranes were blocked for 1 h with a mixture of 50% Odyssey block buffer (LI-COR® Biosciences, Lincoln, NE, USA) and 50% PBS (pH 7.4). Membranes were incubated overnight in PBS + 0.1% Tween: Odyssey block (1:1) with primary antibodies at dilutions recommended by the vendors for the mouse polyclonal (1:2000) and monoclonal (1 μg/mL) antibodies. The purified rabbit polyclonal antibody was tested at a dilution of 1:4000. Membranes were washed four times with PBS + 0.1% Tween and then incubated with the secondary antibody (Alexa Fluor 680 goat anti-rabbit or Alexa Fluor 680 rabbit anti-mouse IgG, Invitrogen Corporation, Eugene, OR) at a 1:4000 dilution for 1 h. Membranes were again washed four times with PBS + 0.1% Tween, then rinsed and stored in PBS. Membranes were scanned using an Odyssey Infared Imaging System.

2.9. Detection of CYP26A1 and CYP26B1 in human tissues

Tissue homogenates were prepared from adipose, kidney, lung, pancreas, skin, spleen and uterus samples purchased from Analytical Biological Services, Inc. (Wilmington, DE). Details of the tissue donor's history are shown in Table 1. Approximately 250 mg of tissue was homogenized in 1 mL of buffer containing 50 mM KPi, 20% glycerol, 1 mM EDTA and protease inhibitors. Homogenization was performed using an Omni homogenizer and corresponding hard tissue disposable grinding tips (Omni International, Marietta, GA). Human liver and human intestinal microsomes were a generous gift from Dr. Catherine K. Yeung, University of Washington, Department of Medicinal Chemistry and were prepared from human liver and intestinal samples obtained from the University of Washington, School of Pharmacy Human Tissue

Table 1
Characteristics of the donors for human tissues used for Western blotting. Human tissue samples were purchased from Analytical Biological Services Inc. All tissue donors were Caucasian.

Tissue	Donor	Sex	Age	Cause of death	Other
Adipose	ABS24116430	F	43	Pulmonary embolism	Arteriosclerotic cardiovascular disease
Intestine	In-house	M	27	n/a	n/a
Kidney	ABS26224571	M	57	Myocardial infarction	Untreated prostate cancer, emphysema, diabetic
Lung	ABS05-06033	F	78	Aneurysm	
Pancreas	ABS24014203	M	54	Ventricular tachycardia	Heart disease
Skin	ABS150402109	F	64	Coronary artery disease	Smoker, heavy ethanol use
Spleen	ABS040426	F	79	Cardio-pulmonary collapse	Ovarian cancer-received treatment
Uterus	ABS030033	F	44	Cerebral vascular accident	

Bank (Seattle, WA). Protein concentrations for the homogenates and microsomes were determined using Pierce (Rockford, IL) BCA Protein Assay Reagents. To determine if CYP26B1 is present in human liver, samples from 32 donor livers were blotted and probed using the rabbit polyclonal antibody. A calibration curve containing 0.1–0.5 pmol of purified CYP26A1 or CYP26B1 was included on each gel for reference and to serve as a positive control. A negative control containing 0.2 pmol of the other CYP26 enzyme was also loaded to demonstrate detection specificity. Eighty μg of HLM, human tissue homogenate or intestinal microsomes was loaded per lane on each blot. CYP26A1 was detected using a rabbit polyclonal antibody raised against a C-terminal peptide of CYP26A1, which was peptide affinity purified and validated as described previously [25]. Western blots were performed using the same procedure used to validate the antibodies. Alexa Fluor 680 goat anti-rabbit antibody was used as the secondary antibody.

2.10. General incubation, extraction, and HPLC analysis protocol

Incubation and extraction of *at*RA and its metabolites, followed by HPLC analysis, was performed as previously described [25]. Standard curves were constructed for *at*RA, 4-OH-RA, 18-OH-RA and 4-oxo-RA to allow quantification of these compounds. P450 reductase was added to CYP26A1 and CYP26B1 membrane preparations in a 2:1 reductase to P450 ratio at room temperature and left for 5 min for reductase incorporation into the membrane. KPi buffer was added to make the incubation volume 1 mL, and 10 μL of substrate in ethanol was added. All experiments were performed under red light. Samples were pre-incubated for 5 min before initiating the reaction with 1 mM NADPH. Incubations were terminated with 3 mL of ethyl acetate and, for quantitative assays acitretin (10 μL of a 5 μM solution) was added as an internal standard. The ethyl acetate layer was evaporated and the dry residue was reconstituted in 100 μL of methanol. Analytes were separated using an Agilent Technologies (Palo Alto, CA) 1200 series HPLC system and detected with a multiple wavelength detector at 360 nm as previously described [25]. Data were analyzed using Agilent ChemStation software. All product formation was confirmed to be dependent on NADPH.

2.11. Identification of metabolites formed by CYP26A1 and CYP26B1 from atRA

To identify the metabolites formed from *at*RA by CYP26A1 and CYP26B1, *at*RA and *at*RA-d_5 (100 μM) were incubated with 100 pmol of each CYP26 isoform and 200 pmol of reductase for 1 h. In addition, 4-OH-RA, 18-OH-RA and 4-oxo-RA were incubated with 50 pmol of CYP26A1 and CYP26B1, 100 pmol of reductase and 10 μM of substrate and the products were analyzed by LC–MS/MS. The incubation mixtures were extracted with ethyl acetate (no internal standard added) and analyzed using an AB Sciex API 5500 Q/LIT mass spectrometer equipped with an Agilent 1290 Infinity UPLC and Agilent Zorbax C18 column (3.5 μm, 2.1 mm × 100 mm) using a method adapted from previous study with *9-cis*-RA metabolites [12]. The metabolites were separated using gradient elution from 10% acetonitrile and 90% aqueous ammonium acetate (50 mM) to 90% acetonitrile over 30 min. The column was maintained at 25 °C and the injection volume was 2 μL. Metabolites were monitored by negative ion electrospray mass spectrometry with the ion source voltage and source temperature set at −4500 V and 400 °C, respectively. The parent-fragment MS/MS transitions (SRM transitions) of m/z 313 > 269 Da, m/z 315 > 241 Da, m/z 315 > 253 Da, m/z 329 > 255 Da, m/z 329 > 267 Da, 331 > 239 Da and m/z 331 > 269 Da were monitored in incubations with unlabeled *at*RA and its metabolites. From incubations with *at*RA-d_5, SRM transitions of m/z 316 > 272 Da, m/z 319 > 257 Da, m/z 320 > 246 Da, m/z 331 > 269 Da, 332 > 258 Da, m/z 334 > 272 Da and m/z 335 > 243 Da were monitored. The declustering potential (DP), collision energy (CE) and collision exit potential (CXP) were set to −90 V, −25 V, and −10 V, respectively. The above MRM scan was used as the survey scan (threshold of >1000 cps) for parallel information dependent acquisition via an enhanced product ion (EPI) scan of [M−H] ions: m/z 315, m/z 313, m/z 331, m/z 329 Da, for *at*RA and its metabolite incubations, and m/z 320, m/z 319, m/z 316, m/z 335, m/z 332 and m/z 334 Da for *at*RA-d_5 incubations. The MS/MS spectra were collected from m/z 50 to 350 Da. The detection settings for the EPI scan parameters were identical to those for the SRM transitions except the CE was increased to −35 V with a spread of ±10 V. Formation of all the identified metabolites was determined to be NADPH cofactor dependent.

2.12. Characterization of enzyme kinetic parameters for metabolism of atRA, 4-OH-atRA, 18-OH-atRA and 4-oxo-atRA by CYP26A1 and CYP26B1

The kinetics of formation of 4-OH-RA and 18-OH-RA catalyzed by CYP26A1 and CYP26B1 were determined. Two pmol of CYP26 and 4 pmol of reductase were incubated at room temperature in 1 mL KPi buffer for 5 min to allow for reductase incorporation into the membrane. *at*RA was then added, and samples were incubated at 37 °C in the presence of NADPH for 2 min (CYP26A1) or 5 min (CYP26B1). Products from the incubations were analyzed using HPLC–UV as described [25]. *at*RA concentrations ranged from 10 nM to 250 nM. The depletion of 4-OH-RA, 4-oxo-RA and 18-OH-RA (200 nM initial concentrations) by CYP26A1 and CYP26B1 was analyzed using similar incubation conditions with the incubations scaled up to 4.5 mL. Aliquots (1 mL) were collected from the incubations at 0, 1, 5, 10 and 20 min and analyzed by HPLC–UV. To determine the V_{max} and K_m for formation of 4-OH-RA and 18-OH-RA, the substrate concentration was corrected for depletion, the measured velocities were plotted as a function of *at*RA concentration and the Michaelis–Menten equation fitted to the data using GraphPad Prism v.5 (La Jolla, CA). The depletion rate constant was determined from a mono-exponential decay.

3. Results

3.1. CYP26A1 and CYP26B1 mRNA expression in human tissues

The quantification of expression of CYP26A1 and CYP26B1 mRNA in human tissues is shown in Fig. 2. The expression of CYP26A1 transcripts varied by 66-fold between tissues with absolute copy numbers between 1400 copies in the duodenum and 96,600 copies in the brain per μg of total RNA. CYP26A1 mRNA was below the limit of quantification for bladder, colon, ileum, and skin although it was detected in the skin. CYP26B1 transcript expression was quantifiable in all tissues tested and varied by 52-fold. Absolute copy numbers ranged from 11,000 copies in the colon to 574,000 copies in the cerebellum per μg of total RNA. Overall CYP26B1 mRNA expression was more ubiquitous than CYP26A1 and, with the exception of the lung and the liver, CYP26A1 transcript amounts did not exceed CYP26B1. However, a significant correlation (p-value 0.01) was observed between the CYP26A1 and CYP26B1 mRNA expression in the tissues studied (Fig. 2c). This correlation was not due to overall correlation in mRNA quality between the tissues since no correlation between CYP26A1 or CYP26B1 with other retinoid related genes such as RAR isoforms, cellular retinoic acid binding proteins (CRABPs) or PPARs was detected (data not shown).

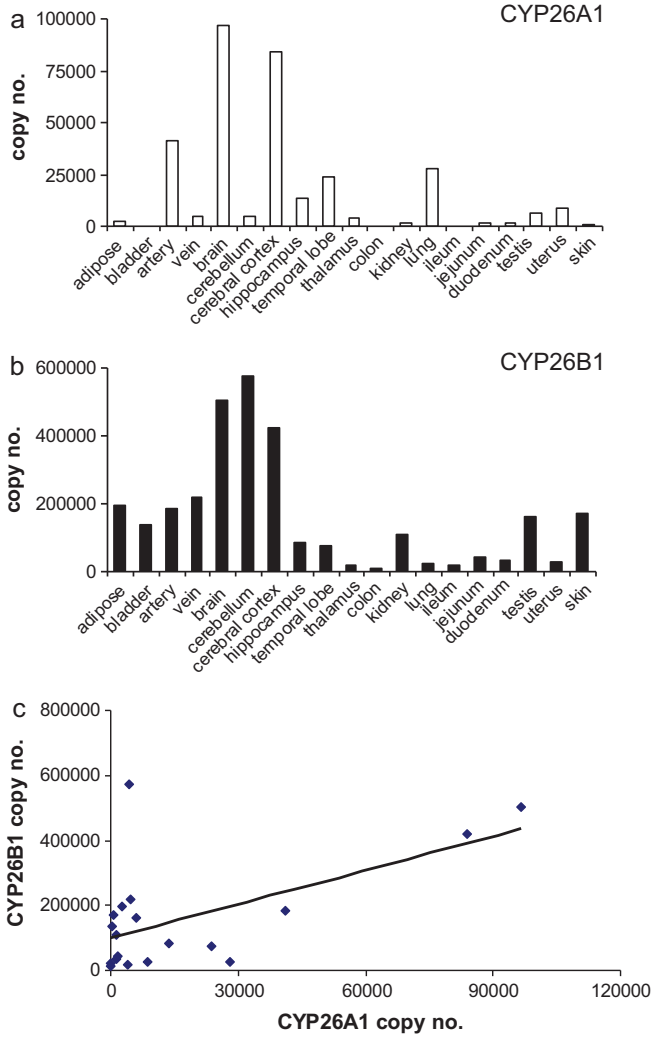

Fig. 2. CYP26A1 and CYP26B1 mRNA expression in human tissues. CYP26A1 (a) and CYP26B1 (b) mRNA copy numbers were determined by real-time PCR in 19 human tissues. The correlation between CYP26A1 and CYP26B1 mRNA in adult tissues is shown in panel (c). mRNA was quantified using absolute quantification as described in Section 2.3.

3.2. Detection of CYP26A1 and CYP26B1 in human tissues

To determine the expression of CYP26A1 and CYP26B1 protein in human tissues, a selective antibody for CYP26B1 was identified. The specificity and sensitivity of three available CYP26B1 antibodies was tested using CYP26B1 and CYP26A1 microsomal preparations and a panel of Supersomes of 10 common drug metabolizing P450s. All CYP26B1 antibodies detected CYP26B1 and did not cross-react with CYP26A1 (Fig. 3A–C), but weak cross reactivity with other P450 isoforms and lower molecular weight interference was detected with the mouse monoclonal and polyclonal antibodies. Therefore the rabbit polyclonal antibody was selected to detect CYP26B1 expression in human tissues.

In the 32 human livers tested, CYP26B1 was not detected in any of the samples although purified CYP26B1 was detectable on all blots (Fig. 3D). Hence, CYP26B1 expression in human liver is below 0.1 pmol per 80 μg of microsomes. CYP26A1 and CYP26B1 proteins were both detected in all eight other human tissues tested (Fig. 3E). The expression of CYP26A1 and CYP26B1 was highest in the pancreas, lung and uterus followed by the skin. Weak expression of CYP26A1 and CYP26B1 was detected in the kidney, spleen, adipose and intestine. Similar to the mRNA expression data, CYP26A1 and CYP26B1 expression correlated between adult tissues.

3.3. Expression of recombinant CYP26B1

To characterize the catalytic activity and function of CYP26B1 a recombinant expression system was developed. CYP26B1 microsomes, prepared from the CYP26B1 baculovirus infected Sf9 cells displayed a classic CO difference spectrum with a defined peak at 450 nm, whereas mock infected control preparation did not show a peak at 450 nm (data not shown). The average expression level of CYP26B1 in the crude Sf9 cells was 30–40 nmol/L. The specific P450 content of the CYP26B1 membrane preparation was 0.079 nmol/mg protein. In preliminary incubations, CYP26B1 was found to metabolize *at*RA to several products including 4-OH-RA. The formation of these products was dependent on NADPH and P450 (data not shown). No product formation was observed in incubations with microsomes from mock-infected cells supplemented with P450 reductase, in incubations without NADPH or in incubations without substrate (*at*RA). To further characterize the recombinant CYP26B1, it was solubilized using NP40 and cholate, and purified using metal affinity chromatography. The CO-difference spectrum and the absolute spectrum of the purified CYP26B1 are shown in Fig. 4A and B. The purified protein was determined to have the correct molecular weight (~56 kDa) based on gel electrophoresis. The binding of *at*RA to CYP26B1 was confirmed by difference spectroscopy. Binding of *at*RA with CYP26B1 resulted in a type I difference spectrum indicating a low-to-high spin shift of the heme iron (Fig. 4C). The magnitude of the difference spectrum was *at*RA concentration dependent and indicated tight binding of *at*RA with CYP26B1 (Fig. 4C).

3.4. Identification of primary metabolites formed from atRA by CYP26B1

When *at*RA and *at*RA-d_5 were incubated with CYP26B1, three primary hydroxylation products ($[M-H]^-$ m/z 315 Da from *at*RA incubations and m/z 319 or 320 Da for *at*RA-d_5 incubations) and a secondary oxidation product (aldehyde or ketone with $[M-H]^-$ ion of m/z 313 and m/z 316 Da from *at*RA and *at*RA-d_5, respectively) were detected by LC–MS/MS (Fig. 5 and Table 2). A similar profile of

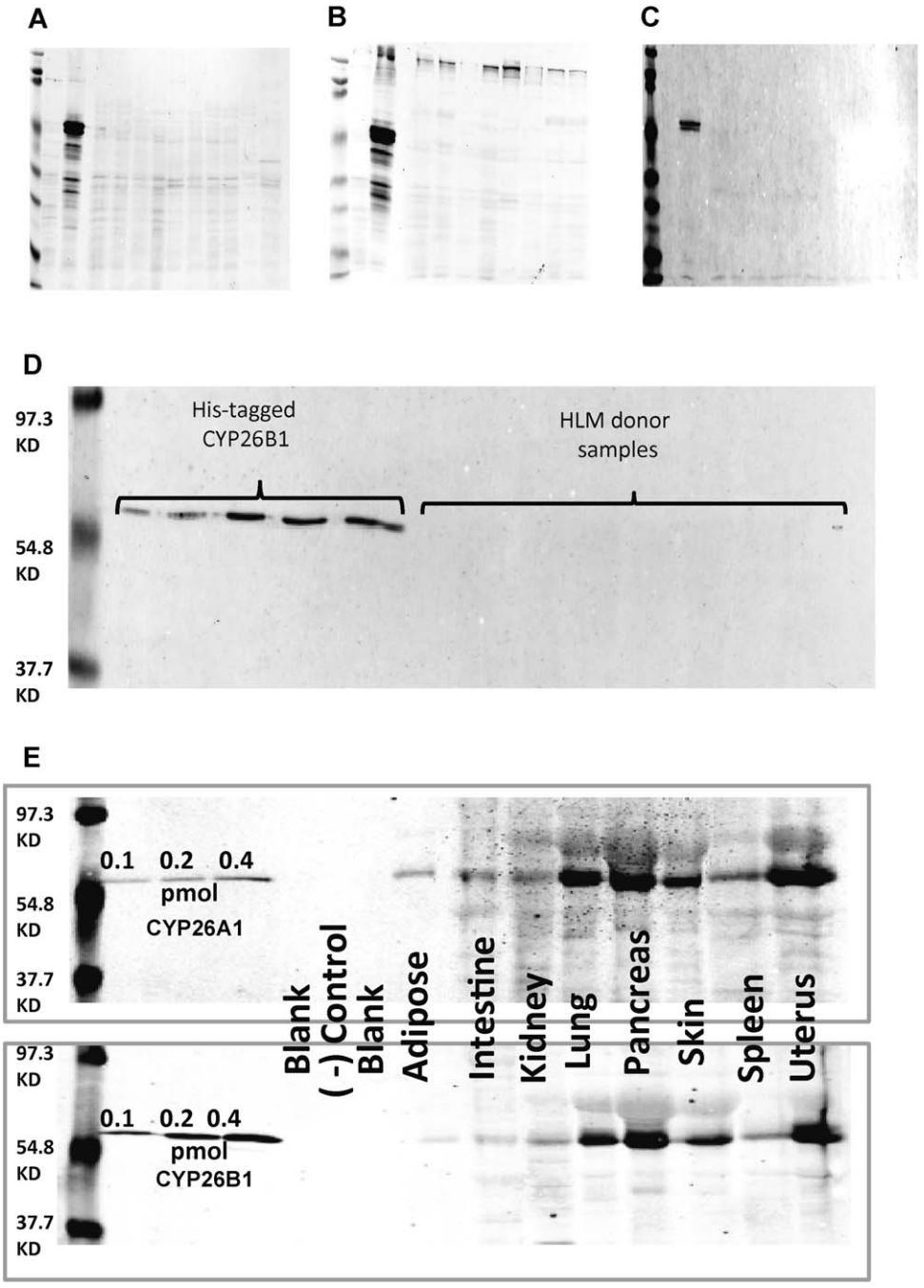

Fig. 3. Detection of CYP26A1 and CYP26B1 in human tissues by Western blot. Panels A (mouse polyclonal CYP26B1 antiserum), B (mouse monoclonal CYP26B1 antibody) and C (rabbit polyclonal purified CYP26B1 antibody) show the evaluation of the three antibodies against recombinant P450 supersomes. The order of the lanes in panels A, B and C is as follows: marker, 5 μg CYP26A1 microsomes, 10 μg of CYP26B1 membrane preparation, blank, and 20 μg of CYP1A1, CYP1A2, CYP2C8, CYP2C9, CYP2C18, CYP2C19, CYP2D6, CYP3A4, CYP3A5, and CYP3A7 supersomes. Panel D shows a representative Western blot of human liver samples probed for CYP26B1 expression. CYP26B1 protein was detected in the 0.1–0.5 pmol standards, but not in any of the HLM samples. Panel E shows a representative detection of CYP26A1 and CYP26B1 in human tissue homogenates. As a negative (−) control, 0.2 pmol of CYP26A1 was loaded on the gel run for CYP26B1 and vice versa showing lack of cross reactivity of the used antibodies.

metabolites was observed from incubations of *at*RA with CYP26A1 (Table 3). The MS/MS data of the major metabolites detected from incubations of *at*RA with CYP26B1 and CYP26A1 are summarized in Tables 2 and 3, respectively. Due to the locations of the 5 deuteriums at C-4 and C-18 in *at*RA-d_5 (Fig. 1), comparison of the LC–MS data between *at*RA and *at*RA-d_5 incubations allowed identification of 4-OH-RA and 18-OH-RA as metabolites of *at*RA formed by CYP26B1 (Fig. 5). The hydroxylation sites were confirmed by comparison of the retention times and fragmentation patterns of the metabolites to reference standards.

The third hydroxylation product formed by CYP26B1 was identified as 16-OH-RA based on similar MS/MS fragmentation pattern as previously reported [12] and the fact that it retained all five deuteriums after hydroxylation (Fig. 5). The metabolite with an $[M-H]^-$ ion at m/z 313 Da from incubations of *at*RA with CYP26A1 and CYP26B1 was identified as 4-oxo-RA based on the loss of two deuteriums from the incubations with *at*RA-d_5, the retention time that was identical with the synthetic reference material, and the MS/MS fragmentation pattern similar to the reference material (Fig. 5 and Tables 2 and 3).

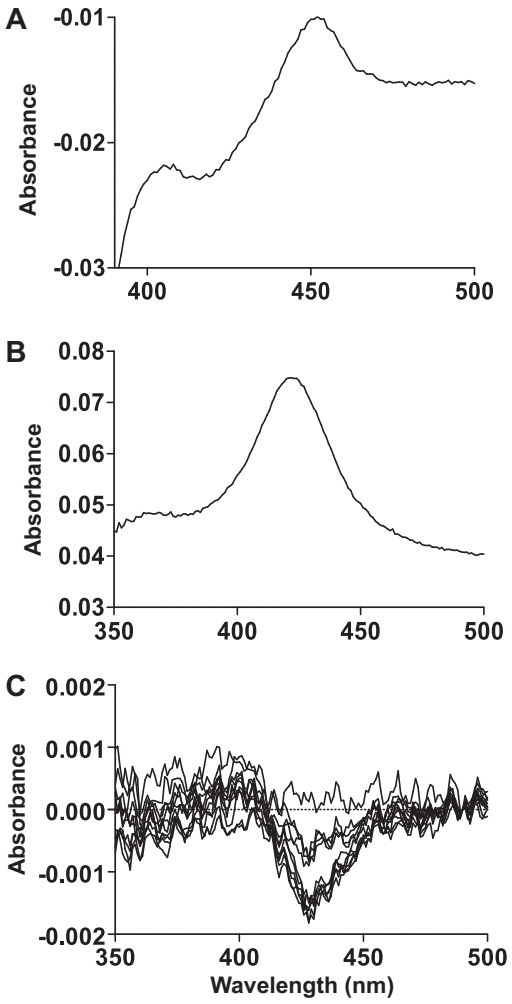

Fig. 4. Characterization of the recombinant CYP26B1. CYP26B1 was expressed in Sf9 cells, solubilized as described in Section 2.6 and then purified using a talon affinity column. Panel A shows a CO-difference spectrum of the purified CYP26B1, panel B shows the absolute spectrum of the purified CYP26B1 and panel C shows the difference spectrum of CYP26B1 in the presence of increasing concentrations of *at*RA (10–500 nM).

3.5. Kinetics of formation to 4-OH-RA and 18-OH-RA by CYP26A1 and CYP26B1 and depletion of 4-OH-RA, 18-OH-RA and 4-oxo-RA by CYP26A1 and CYP26B1

The formation kinetics of 4-OH-RA and 18-OH-RA was measured for CYP26A1 and CYP26B1. The Michaelis–Menten plots and HPLC–UV chromatograms of the kinetic characterization are shown in Fig. 6. Based on 4-OH-RA formation, CYP26A1 had greater catalytic activity (V_{max}) than CYP26B1 but lower affinity for *at*RA than did CYP26B1 (Table 4). Based on the HPLC–UV traces, 4-OH-RA was the most abundant metabolite formed by both enzymes (Fig. 6A and B). The predominant formation of 4-OH-RA was also supported by the 45% lower V_{max} for 18-OH-RA formation compared to 4-OH-RA formation by CYP26A1. With CYP26B1, 18-OH-RA formation could be detected but the formation was insufficient to determine kinetic constants. Based on the overall intrinsic clearances, CYP26A1 has a significantly higher catalytic efficiency towards *at*RA than does CYP26B1.

In incubations of *at*RA with CYP26A1 and CYP26B1, metabolites that were more polar than 4-OH-RA were detected (Fig. 6A and B) suggesting that some primary oxidation products of *at*RA are also substrates of CYP26A1 and CYP26B1. Indeed, when 4-OH-RA, 18-OH-RA and 4-oxo-RA were incubated with CYP26A1 and CYP26B1 depletion of all three substrates was observed (Fig. 7), and formation of more polar metabolites detected (Fig. 8). The depletion rates of 4-OH-RA, 18-OH-RA and 4-oxo-RA were determined in incubations of 200 nM of each as substrate with CYP26A1 and CYP26B1 (Table 5 and Fig. 7). CYP26A1 had higher catalytic activity and faster depletion rates (0.05–0.12 min^{-1}) towards all the metabolites than did CYP26B1 (0.02–0.03 min^{-1}). Interestingly, CYP26B1 depleted all three metabolites with similar efficiency, whereas CYP26A1 had twice the catalytic activity towards the primary hydroxylation products than towards 4-oxo-RA (Table 5).

3.6. Identification of sequential metabolites from atRA and metabolites of 4-OH-RA, 4-oxo-RA and 18-OH-RA formed by CYP26A1 and CYP26B1

To characterize the sequential metabolites formed from *at*RA by CYP26, *at*RA, *at*RA-d_5, 4-OH-RA, 18-OH-RA and 4-oxo-RA were incubated with CYP26A1 and CYP26B1 and metabolite formation was determined by LC–MS/MS. Three metabolites with $[M-H]^-$ ions at *m*/*z* 331 Da and two metabolites with $[M-H]^-$ ions at *m*/*z* 329 Da were detected (Fig. 8, Tables 2 and 3). The first metabolite with an $[M-H]^-$ of *m*/*z* 331 Da at retention time 10.4 min was formed by CYP26A1 and CYP26B1 from 4-OH-RA and *at*RA but not from 18-OH-RA or 4-oxo-RA as substrates (Fig. 8). This product showed loss of only one deuterium atom when *at*RA-d_5 was the substrate (Tables 2 and 3). The MS/MS fragmentation pattern of this metabolite showed a major fragment at *m*/*z* 239 Da that was proposed to result from loss of CO_2 (−44 Da), formaldehyde (−30 Da) and water (−18 Da) supporting identification of this metabolite as 4,16-$(OH)_2$-RA. The metabolite at retention time 13.7 min ($[M-H]^-$ *m*/*z* 331 Da) was formed from *at*RA, 4-OH-RA and 18-OH-RA by CYP26B1 and CYP26A1 (Fig. 8, Tables 2 and 3). This metabolite was identified as 4,18-$(OH)_2$-RA because it lost two deuterium atoms from *at*RA-d_5 suggesting that both hydroxylations occurred at the deuterated carbons C-4 and C-18, and the fragmentation pattern was characterized by the combined loss of CO_2 and water (−44 Da and −18 Da) and subsequent loss of water. The third metabolite with an $[M-H]^-$ *m*/*z* 331 Da eluting at 12.3 min was formed from both 4-OH-RA and 18-OH-RA by CYP26A1 and CYP26B1 but could not be unequivocally identified. Three metabolites with $[M-H]^-$ *m*/*z* 329 Da were detected from the incubations of *at*RA and its metabolites (Fig. 8). The first one with retention time of 12.3 min was formed from *at*RA, 4-OH-RA and 4-oxo-RA by both CYP26A1 and CYP26B1, but was absent in the incubations of 18-OH-RA suggesting that this compound contained the 4-oxo functionality. From the incubations with *at*RA-d_5, this metabolite retained three deuteriums (Tables 2 and 3) suggesting that C-18 was not oxidized. The metabolite showed a major fragment at *m*/*z* 255 Da most likely resulting from the loss of CO_2 (−44 Da) and formaldehyde (−30 Da). Collectively these data support identification of this metabolite as 4-oxo-16-OH-RA. The metabolite with $[M-H]^-$ *m*/*z* 329 Da at retention time 13.8 min was mainly detected from incubations with CYP26A1 (Fig. 8), and it was formed from 4-OH-RA, 18-OH-RA and 4-oxo-RA, suggesting this metabolite results via a convergent pathway from 4-OH-RA, 4-oxo-RA and 18-OH-RA. Since it has a 4-oxo-functionality, this metabolite was identified as 4-oxo-18-OH-RA. An additional metabolite with $[M-H]^-$ 329 *m*/*z* was detected from incubations of *at*RA, 18-OH-RA and 4-OH-RA but not from 4-oxo-RA with CYP26A1 and CYP26B1 at retention time 14.2 min (Tables 2 and 3 and Fig. 8). Based on the data, this metabolite may be 18-oxo-4-OH-RA. Due to an isotope effect on C-18 oxidation, this metabolite was, however, not sufficiently abundant from incubations of *at*RA-d_5, to provide MS/MS spectra. Formation of an 18-oxo-RA metabolite was further supported by the observation of a

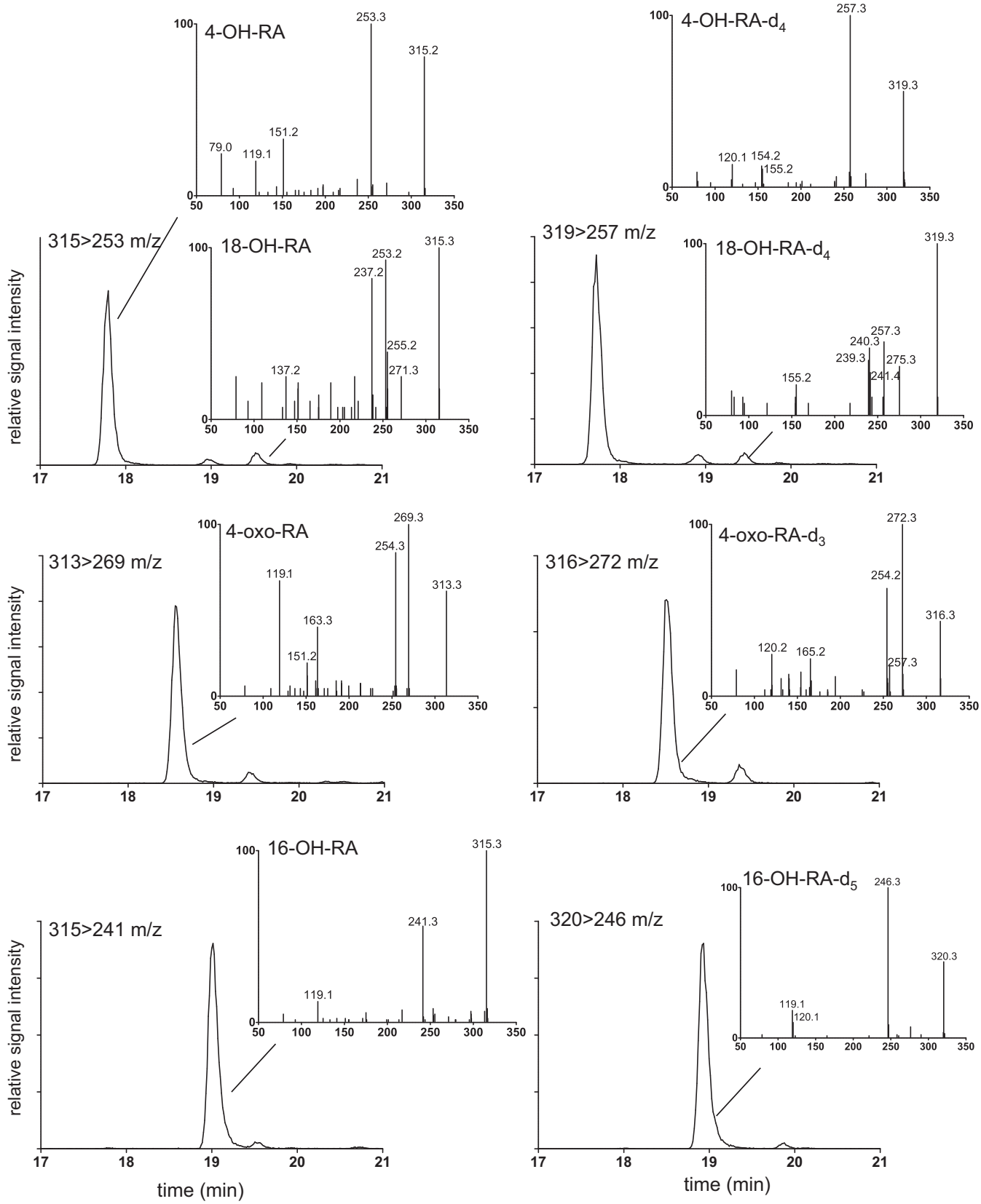

Fig. 5. Identification of primary metabolites of *at*RA formed by CYP26B1. CYP26B1 was incubated with *at*RA and *at*RA-d_5 and SRM chromatograms as well as MS/MS fragmentation patterns were collected as described in Section 2.11. The left panel shows the MS/MS spectra and SRM chromatograms collected in incubations with *at*RA and right panel shows the corresponding data collected from incubations with *at*RA-d_5 with CYP26B1. Each inset depicts the MS/MS spectrum of the chromatographic peak indicated. The inset on each panel lists the SRM transition depicted and the identified metabolite from that SRM transition. The metabolites were identified as 4-OH-*at*RA; 4-oxo-*at*RA; 16-OH-*at*RA and 18-OH-*at*RA as indicated for each panel.

Table 2
Summary of the MS/MS fragmentation patterns of *at*RA and *at*RA-d_5 metabolites formed by CYP26B1. The metabolites that are also oxidized to the same products when incubated separately with CYP26B1 are listed in the last column. The five most abundant fragments that were also ≥10% abundance are shown.

Metabolite	rt (min)	Parent *m/z*	Fragment *m/z* (% abundance)	Formed from
*at*RA incubation				
4,16-$(OH)_2$-RA	10.4	331	239 (86), 201 (31), 137 (31), 119 (41), 79 (10)	4-OH-RA
$(OH)_2$-RA	12.3	331	257 (12), 239 (100), 201 (25), 137 (13), 119 (32)	4-OH-RA
4-oxo-16-OH-RA	12.3	329	255 (100), 171 (16), 137 (30), 135 (26), 119 (24)	4-OH-RA and 4-oxo-RA
4,18-$(OH)_2$-RA	13.7	331	269 (45), 251 (50), 177 (24), 149 (20), 137 (27)	4-OH-RA and 18-OH-RA
oxo-OH-RA	14.2	329	269 (50), 267 (100), 131 (92), 119 (50), 97 (42)	4-OH-RA and 18-OH-RA
4-OH-RA	17.8	315	253 (100), 151 (33), 119 (21), 79 (24)	
4-oxo-RA	18.6	313	269 (100), 254 (83), 163 (41), 151 (19), 119 (67)	4-OH-RA
16-OH-RA	19.0	315	241 (57), 119 (12)	
18-OH-RA	19.5	315	271 (25), 255 (40), 253 (92), 237 (83), 137 (25)	
*at*RA-d_5 incubation				
4,16-$(OH)_2$-RA	10.4	335	243 (100), 204 (14), 141 (11), 119 (22)	
$(OH)_2$-RA	12.3	335	261 (13), 243 (100), 204 (24), 119 (30), 79 (14)	
4,18-$(OH)_2$-RA	13.6	334	272 (45), 258 (23), 254 (22), 138 (27), 79 (23)	
4-OH-RA	17.7	319	257 (100), 155 (11), 154 (14), 120 (13)	
4-oxo-RA	18.5	316	272 (100), 257 (18), 254 (63), 165 (22), 120 (24)	
16-OH-RA	18.9	320	246 (100), 120 (11), 119 (18)	
18-OH-RA	19.5	319	275 (28), 257 (42), 241 (25), 240 (40), 239 (33)	

metabolite with $[M-H]^-$ ion at *m/z* 313 Da at retention time 21 min from *at*RA and 18-OH-RA (Fig. 9A and C). This metabolite also lost two deuteriums from *at*RA-d_5 (Fig. 9B) but was not formed from 4-OH-RA or 4-oxo-RA and had a distinct fragmentation pattern when compared to 4-oxo-RA. An additional metabolite with $[M-H]^-$ of *m/z* 329 Da at retention time of 13.5 min was detected in incubations of 18-OH-RA with CYP26A1 and CYP26B1 (Fig. 8). The MS/MS spectrum of this metabolite was dominated by a major fragment at *m/z* 255 Da and minor fragments at *m/z* 299, *m/z* 281, *m/z* 237 and *m/z* 211 Da. However, the oxidation site in this metabolite could not be determined from the available data.

4. Discussion

The CYP26A1 and CYP26B1 mRNA and protein quantification in human tissues suggests that their expression is overlapping in adult tissues. The detection of CYP26A1 and CYP26B1 mRNA is consistent with previously published data showing that they have broad tissue distribution [15,24]. Qualitatively the detection of CYP26A1 and CYP26B1 mRNA in adipose tissue, intestine, kidney, lung, skin and uterus is also in agreement with the detection of CYP26A1 and CYP26B1 protein in these tissues. However, the quantitative rank order of CYP26 mRNA abundance did not predict the highest protein expression tissues. For example, CYP26B1 mRNA was much more abundant in the kidney than in the lung but CYP26B1 protein expression was greater in the lung than in the kidney. For CYP26A1, the rank order of mRNA abundance seemed to be a better predictor of protein abundance than for CYP26B1. The discrepancy between mRNA and protein is most likely due to inter-individual variability between donors since the same donors were not available for mRNA and protein quantification. Large inter-individual variability in CYP26A1 mRNA and protein expression has been shown previously in a panel of human livers [25], and can be expected in other tissues as well. Based on studies performed in rodents [33], it is also likely that CYP26 expression in humans changes with age or in response to environmental factors. Therefore large banks of tissues should be characterized to determine the importance of CYP26 isoforms in specific adult tissues such as the pancreas, lung and brain regions.

Significant correlation in the expression of the two CYP26 isoforms has not been observed previously and is in contrast to the distinct tissue and developmental stage specific expression of CYP26A1 and CYP26B1 during fetal development [19,34,35]. The correlation in adult tissues is also of interest since no apparent

Table 3
Summary of the MS/MS fragmentation patterns of *at*RA and *at*RA-d_5 metabolites formed by CYP26A1. The metabolites that are also oxidized to the same products when incubated separately with CYP26A1 are also listed in the last column. The five most abundant fragments that were also ≥10% abundance are shown.

Metabolite	rt (min)	Parent *m/z*	Fragment *m/z* (% abundance)	Formed from
*at*RA incubation				
4,16-$(OH)_2$-RA	10.4	331	257 (18), 239 (99), 201 (37), 137 (19), 119 (46)	4-OH-RA
$(OH)_2$-RA	12.3	331	255 (69), 239 (100), 201 (17), 137 (26), 119 (49)	4-OH-RA
4-oxo-16-OH-RA	12.3	329	255 (100), 240 (19), 211 (14), 137 (16), 135 (24)	4-OH-RA and 4-oxo-RA
4,18-$(OH)_2$-RA	13.7	331	269 (68), 251 (45), 235 (25), 137 (53), 79 (22)	4-OH-RA and 18-OH-RA
4-oxo-18-OH-RA	13.8	329	267 (75), 251 (31), 239 (22), 161 (83), 79 (100)	4-OH-RA, 4-oxo-RA and 18-OH-RA
oxo-OH-RA	14.2	329	267 (100), 229 (58), 163 (75), 161 (92), 131 (83)	4-OH-RA and 18-OH-RA
4-OH-RA	17.8	315	253 (100), 151 (19), 119 (12), 79 (13)	
4-oxo-RA	18.6	313	269 (100), 254 (76), 191 (11), 163 (21), 119 (33)	4-OH-RA
16-OH-RA	19.0	315	241 (100), 119 (25)	
18-OH-RA	19.5	315	271 (38), 253 (82), 241 (17), 237 (67), 151 (36)	
*at*RA-d_5 incubation				
4,16-$(OH)_2$-RA	10.4	335	261 (10), 243 (85), 204 (33), 119 (25), 79 (10)	
$(OH)_2$-RA	12.3	335	243 (100), 204 (30), 140 (13), 119 (42), 79 (13)	
4-oxo-16-OH-RA	12.3	332	258 (100), 243 (11), 178 (12), 140 (20), 138 (20)	
4,18-$(OH)_2$-RA	13.6	334	272 (77), 254 (42), 238 (31), 215 (27), 138 (50)	
4-OH-RA	17.7	319	257 (100), 256 (12), 154 (14)	
4-oxo-RA	18.5	316	272 (100), 257 (27), 254 (82), 165 (19), 120 (34)	
16-OH-RA	18.9	320	246 (100), 119 (12)	
18-OH-RA	19.5	319	275 (32), 258 (14), 257 (89), 240 (36), 239 (22)	

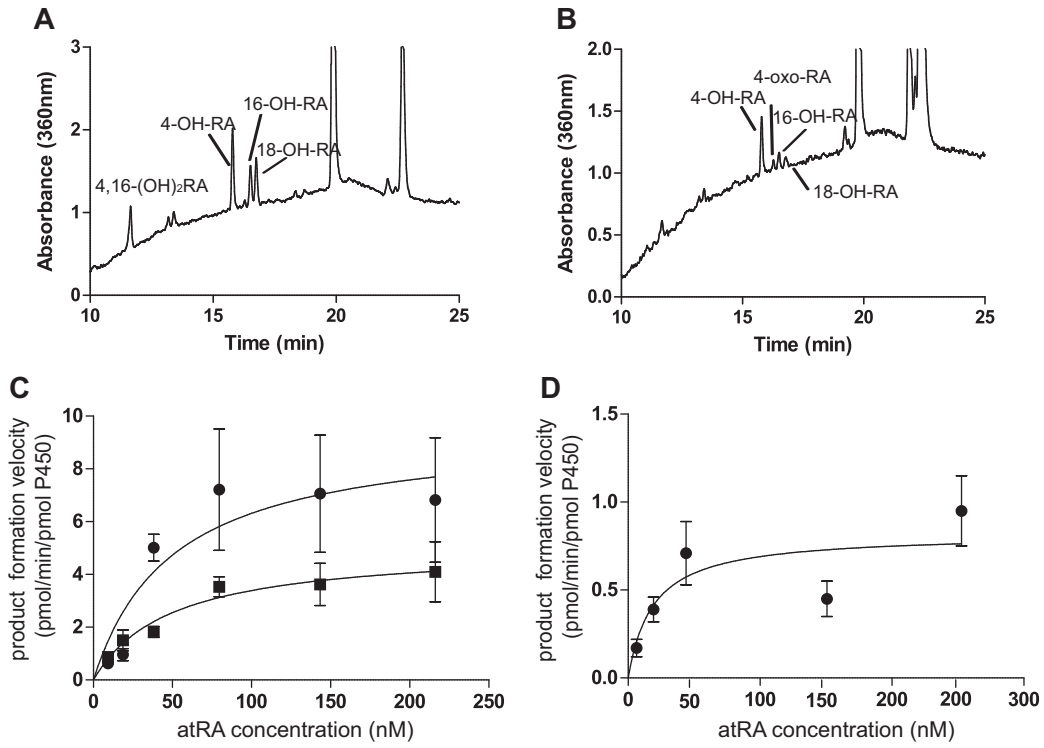

Fig. 6. Determination of kinetics of formation of 4-OH-RA and 18-OH-RA by CYP26A1 and CYP26B1. The formation of 4-OH-RA and 18-OH-RA was determined using 2 pmol CYP26, 4 pmol reductase and *at*RA concentrations of 10–250 nM incubated for 2 min (CYP26A1) or 5 min (CYP26B1). The Michaelis–Menten equation was fitted to the data. Panels A and B show the representative HPLC–UV chromatograms of 4-OH-RA and 18-OH-RA formation by CYP26A1 and CYP26B1, respectively. The Michaelis–Menten plots are shown for CYP26A1 (C) and CYP26B1 (D) mediated 4-OH-RA (circles) and 18-OH-RA (squares) formation.

Table 4
Kinetic parameters determined for 4-OH-RA and 18-OH-RA formation by CYP26A1 and CYP26B1.

	CYP26A1 4-OH-RA	CYP26A1 18-OH-RA	CYP26B1 4-OH-RA
K_m (nM)	50.1 ± 32.4	48.9 ± 13.4	18.8 ± 18.7
V_{max} (pmol/min/pmol P450)	9.5 ± 2.2	5.0 ± 0.5	0.81 ± 0.2
Cl_{int} (μL/min/pmol P450)	190	102	43

differences in CYP26A1 and CYP26B1 catalytic activity have been observed, and the requirement for the two enzymes has been attributed to different regulation of their expression. For example, in the human liver, CYP26A1 is the predominant CYP26 isoform and CYP26B1 protein cannot be detected, and in HepG2 cells, a model of hepatic CYP26 regulation, CYP26A1 mRNA was induced by *at*RA via RAR activation, whereas CYP26B1 mRNA was regulated by PPAR ligands [23]. The results of this study suggest that in select tissues such as cerebellum and the liver, CYP26A1 and CYP26B1 have different expression patterns but in majority of the tissues both enzymes are expressed. In the lung, CYP26A1 mRNA was slightly higher than CYP26B1 and CYP26A1 protein expression also appeared slightly higher. In contrast, the cerebellum appeared to have a high expression of CYP26B1 mRNA but very low CYP26A1 suggesting that in the cerebellum CYP26B1 is the predominant CYP26 isoform.

The overall lower quantification of CYP26A1 mRNA in comparison to CYP26B1 in the human tissues may indicate either lower constitutive expression of CYP26A1 or significantly lower mRNA stability of CYP26A1. In a previous study, similar mRNA half-lives of CYP26A1 and CYP26B1 were determined in cells [23] suggesting similar mRNA stability, but based on Western blot results shown here CYP26A1 expression appeared higher than CYP26B1 suggesting different mRNA stability. Since CYP26B1 has a lower catalytic activity as an *at*RA hydroxylase than CYP26A1, it is likely that CYP26A1 is the main *at*RA hydroxylase in the tissues in which it is expressed even if its expression is lower than CYP26B1. However, it is possible that CYP26B1 is a high affinity low capacity RA hydroxylase with a specific biological role and CYP26A1 is a lower affinity, higher capacity RA hydroxylase. As shown here, *at*RA binds both CYP26A1 and CYP26B1 with high affinity with 2-fold higher K_m for CYP26A1. However, the V_{max} for CYP26B1 mediated 4-OH-RA formation was only 10% of that determined for CYP26A1. In addition formation of other metabolites was not efficient enough by CYP26B1 to allow determination of kinetic constants. Thus, in the overall depletion of *at*RA, CYP26A1 is approximately 20-fold more efficient than CYP26B1 due to rapid formation of multiple primary metabolites (4-OH-RA, 18-OH-RA and 16-OH-RA). This supports the role of CYP26A1 as a high capacity *at*RA hydroxylase. Interestingly, CYP26A1 was only 2–4-fold more efficient in depleting 4-OH-RA, 18-OH-RA and 4-oxo-RA than CYP26B1. The higher capacity and efficiency of CYP26A1 as an *at*RA hydroxylase compared to CYP26B1 appears consistent with its expression in the human liver where it presumably contributes to the first pass metabolism of *at*RA obtained from the diet [25]. Based on mRNA data, CYP26B1 on the other hand is expressed in tissues with much lower metabolic activity such as cerebellum.

Despite the lower catalytic efficiency of CYP26B1 than CYP26A1, it has approximately 100-fold higher intrinsic clearance towards *at*RA than common drug metabolizing P450s such as CYP3A4 and CYP2C8. The intrinsic clearance of *at*RA metabolism by CYP26B1 was 43 μL/min/pmol P450, whereas the intrinsic clearances by CYP3As and CYP2C8 are 0.2–0.4 μL/min/pmol P450 [25]. It is not clear why CYP26B1 has a much lower V_{max} (0.8 pmol/min/pmol P450) for *at*RA hydroxylation than other P450s (2–5 pmol/min/pmol P450 for CYP3As and CYP2C8, 10 pmol/min/pmol P450 for CYP26A1). It is possible that CYP26B1 is not as well coupled for the P450 cycle as the other P450s or that

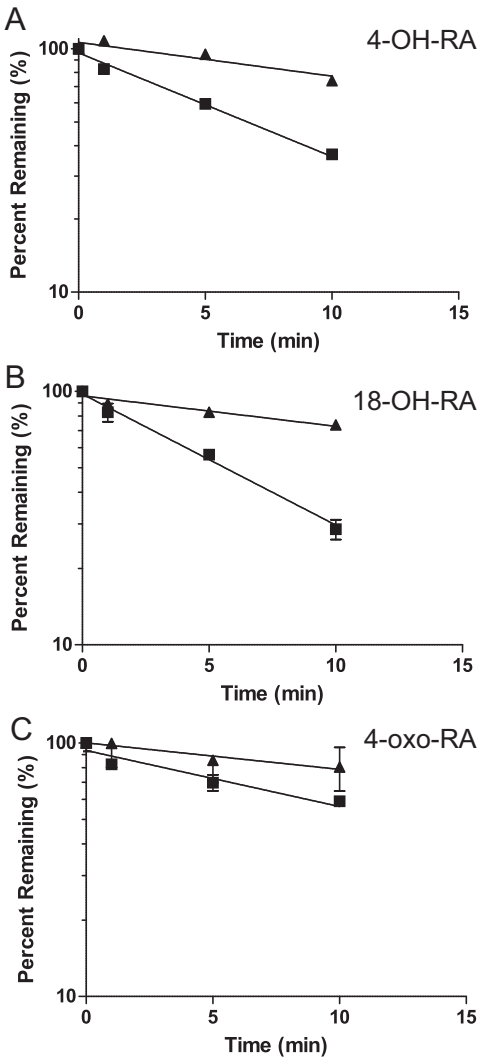

Fig. 7. Depletion kinetics of 4-OH-RA (A), 18-OH-RA (B) and 4-oxo-RA (C) by CYP26A1 and CYP26B1. The depletion time courses for the three metabolites with CYP26A1 (squares) and CYP26B1 (triangles) are shown. The incubations were carried out as described in Section 2.12. A monoexponential decay was fitted to the depletion data to obtain the elimination rate constants.

P450 reductase is not the only electron transfer partner nor the optimal one for CYP26B1. If an alternative electron transfer partner is preferred, the catalytic activity observed in this study does not reflect the maximum catalytic rate of CYP26B1. In addition, the recombinant system used here does not include other cellular soluble or membrane bound proteins. It has been proposed that P450 enzymes obtain *at*RA as a substrate directly from the CRABPs [26]. Since the sequences between the individual CYP26 isoforms are not highly conserved, it is possible that they interact differently with CRABPs via different surface residues. This could affect the relative importance of the two CYP26 isoforms and the catalytic activity.

It is possible that the need for both CYP26A1 and CYP26B1 in adult human tissues is a result of different substrate selectivity or formation of different active metabolites of *at*RA by the two enzymes. The metabolites formed by CYP26A1 and CYP26B1 have not been thoroughly characterized and tested for pharmacological activity. Based on this study, CYP26A1 and CYP26B1 form qualitatively the same primary and sequential metabolites although the 4-OH-RA to 18-OH-RA ratio was greater from CYP26B1 than from CYP26A1. The primary metabolite identification is in agreement with previous report with CYP26A1 [12], and 4-oxo-RA and 18-OH-RA were previously reported as metabolites of *at*RA using COS-1, V79-4 and HeLa cells transfected with CYP26A1 and CYP26B1 [12,14,15]. The relative importance of 4-OH-RA and 16-OH-RA as metabolites of *at*RA cannot be currently determined due to convergent sequential metabolic pathways to 4,16-$(OH)_2$-RA and 4-oxo-16-OH-RA. 16-OH-RA has been identified as the main oxidation product formed by CYP120, the cyanobacterial *at*RA hydroxylase [36]. The 4-oxo-16-OH-RA has also been previously synthesized [37] and shown to bind to cellular retinoic acid binding proteins (CRABPs) [38], but its formation by P450 enzymes has not been demonstrated and its overall biological activity is not known. Whether the sequential oxidation products have a biological function in adult humans requires further study, but it appears that there are no biologically important differences between CYP26A1 and CYP26B1 in the formation of active metabolites.

In the previous study in transfected cells most sequential metabolites had an $[M-H]^-$ ion of 329 m/z suggesting they were oxo-alcohol-compounds [14]. However, the incubations using recombinant CYP26 enzymes show mainly formation of 4,16-$(OH)_2$-RA and 4,18-$(OH)_2$-RA as the sequential metabolites, and oxo-alcohols are observed using 4-oxo-RA as the substrate. Similarly, the 4-oxo-RA metabolite has been shown to be the most abundant metabolite formed from *at*RA in COS-1 cells transfected with CYP26A1 or CYP26B1 [15], whereas 4-oxo-RA is a minor metabolite in incubations of recombinant CYP26s with *at*RA. These differences suggest that formation of oxo-compounds is more abundant in whole cells than in recombinant microsomes. It has previously been shown that a non-NADPH dependent enzyme is mainly responsible for 4-oxo-RA formation [39]. Thus the clearance of *at*RA and its active metabolites appears to involve other enzymes as well as CYP26 isoforms. This divergence of the oxidative metabolism of *at*RA may have biological significance since 4-oxo-RA has been shown to possess biological activity *in vivo* and in cell lines [17,40].

An interesting feature of CYP26A1 and CYP26B1 is that despite their functional similarity as *at*RA hydroxylases, they are only 40–50% identical in overall sequence [11]. The low sequence identity of CYP26 enzymes suggests that CYP26A1 and CYP26B1 would have different catalytic characteristics towards *at*RA. For comparison, the sequence identity between CYP2C8 and CYP2C9 is 70% [41], but only CYP2C8 metabolizes *at*RA efficiently and CYP2C8 and CYP2C9 generally differ in their substrate selectivity and catalytic activities (V_{max} and K_m) and/or metabolite profiles for a given substrate. Based on homology modeling, distinct differences between active site residues in CYP26A1 and CYP26B1 were suggested [42] including more hydrogen bonding interactions in the CYP26B1 active site. This could potentially explain the higher affinity of *at*RA to the CYP26B1 active site observed in this study. However, it does not allow rationalization of the different catalytic rates or the apparent diversity of binding orientations of *at*RA and 4-oxo-RA within the CYP26A1 active site when compared to CYP26B1. Further modeling of CYP26 isoforms to evaluate the binding orientations of *at*RA and its metabolites within the active sites will be valuable in generating more predictive models for design of CYP26 selective inhibitors.

In conclusion, this study is the first report of heterologous expression of CYP26B1 and kinetic characterization of sequential

Table 5
Depletion kinetics 4-OH-RA, 4-oxo-RA and 18-OH-RA by CYP26A1 and CYP26B1.

RA Metabolite	k_{dep} (min^{-1})	
	CYP26A1	CYP26B1
4-OH-RA	0.10 ± 0.01	0.03 ± 0.01
18-OH-RA	0.12 ± 0.01	0.03 ± 0.01
4-oxo-RA	0.05 ± 0.01	0.02 ± 0.00

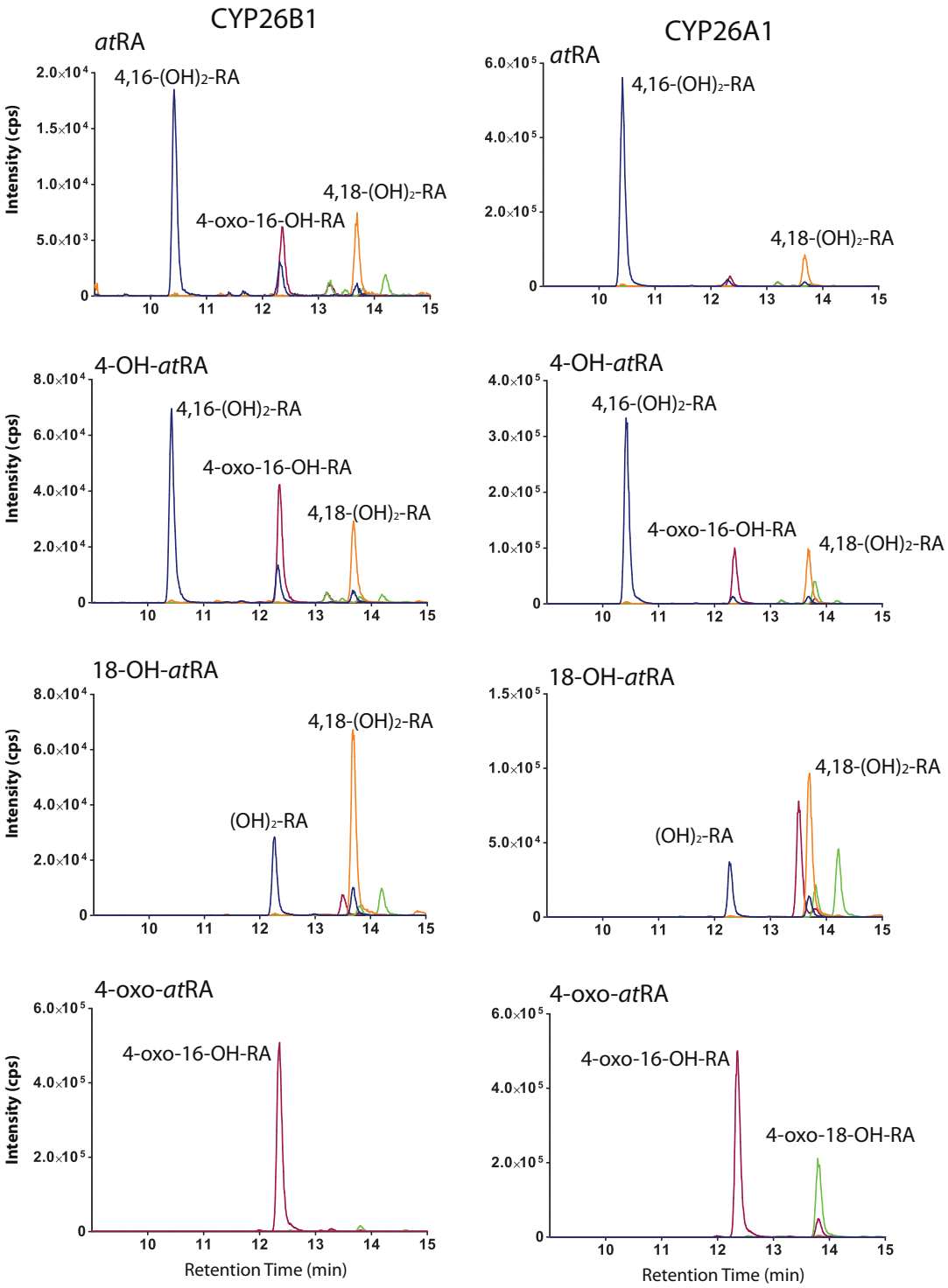

Fig. 8. Identification of sequential metabolites of *at*RA formed by CYP26A1 and CYP26B1. The traces of the SRM transitions of incubations of *at*RA, 4-OH-RA, 18-OH-RA and 4-oxo-RA with CYP26B1 (left panel) and CYP26A1 (right panel) are shown. The substrates were incubated as described in Section 2.11 and the substrate for each panel is listed in the figure. The MS/MS spectral details of the detected peaks are summarized in Tables 1 and 2. The blue traces depict SRM transition 331 > 239 *m/z*, red traces depict SRM transition 329 > 255 *m/z*, yellow traces depict SRM transition 331 > 269 *m/z* and green traces depict 329 > 267 *m/z*. The identification of the metabolites formed is shown in the chromatograms.

metabolism of *at*RA by CYP26B1. The purified CYP26B1 demonstrated a classic P450 spectrum as well as an absolute spectrum characteristic of a P450 enzyme. RA binding within the CYP26B1 active site was shown via difference spectrum of a typical low to high spin shift of the heme following ligand binding. The presented data show that CYP26A1 and CYP26B1 are both efficient hydroxylases of *at*RA and are likely to contribute significantly to *in vivo* clearance of *at*RA. The data indicate that CYP26A1 and CYP26B1 have broad expression in human tissues but CYP26B1 has lower catalytic activity than CYP26A1. In specific tissues such as the cerebellum and liver only one CYP26 isoform appears to be required and further studies in different human tissues are needed to determine the overall importance of the CYP26 enzymes during adult life. The similar metabolic profiles of CYP26A1 and CYP26B1

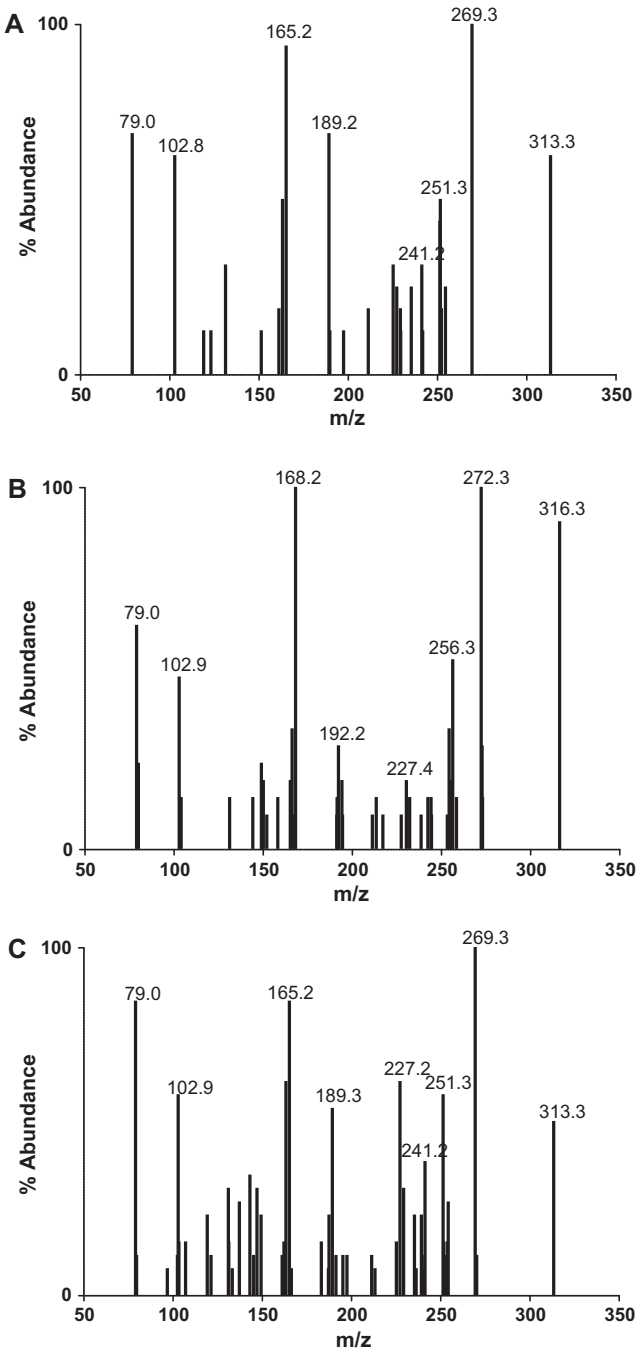

Fig. 9. Mass spectrometric characterization of the 18-oxo-RA metabolite. The MS/MS spectra of parent ion $[M-H]^-$ at 313 *m/z* (A and C) or 316 *m/z* (B) obtained at retention time 21 min from incubation of *at*RA with CYP26A1 (A), *at*RA-d_5 with CYP26A1 (B) and 18-OH-RA with CYP26B1 (C) are shown.

suggest that it will be difficult to differentiate the importance of individual CYP26 isoforms in maintaining retinoic acid homeostasis *in vivo*.

Acknowledgments

This work was supported by National Institute of General Medical Sciences grants T32 GM007750, R01 GM081569 and R01 GM081569-S1 as well as The NIH National Center of Research Resources grant TL1 RR025016. The authors wish to thank Dr Leslie Dickmann for her help in the initial evaluation of CYP26B1 expression and for helpful discussions during this work.

References

[1] Altucci L, Leibowitz MD, Ogilvie KM, de Lera AR, Gronemeyer H. RAR and RXR modulation in cancer and metabolic disease. Nat Rev Drug Discov 2007;6:793–810.
[2] Mark M, Ghyselinck NB, Chambon P. Function of retinoid nuclear receptors: lessons from genetic and pharmacological dissections of the retinoic acid signaling pathway during mouse embryogenesis. Annu Rev Pharmacol Toxicol 2006;46:451–80.
[3] Noy N. Between death and survival: retinoic acid in regulation of apoptosis. Annu Rev Nutr 2010;30:201–17.
[4] White JC, Shankar VN, Highland M, Epstein ML, DeLuca HF, Clagett-Dame M. Defects in embryonic hindbrain development and fetal resorption resulting from vitamin A deficiency in the rat are prevented by feeding pharmacological levels of all-trans-retinoic acid. Proc Natl Acad Sci USA 1998;95:13459–64.
[5] Collins MD, Tzimas G, Hummler H, Burgin H, Nau H. Comparative teratology and transplacental pharmacokinetics of all-trans-retinoic acid, 13-cis-retinoic acid, and retinyl palmitate following daily administrations in rats. Toxicol Appl Pharmacol 1994;127:132–44.
[6] Shudo K, Fukasawa H, Nakagomi M, Yamagata N. Towards retinoid therapy for Alzheimer's disease. Curr Alzheimer Res 2009;6:302–11.
[7] Maden M. Retinoic acid in the development, regeneration and maintenance of the nervous system. Nat Rev Neurosci 2007;8:755–65.
[8] Blomhoff R, Blomhoff HK. Overview of retinoid metabolism and function. J Neurobiol 2006;66:606–30.
[9] Ross AC, Zolfaghari R. Cytochrome p450s in the regulation of cellular retinoic acid metabolism. Annu Rev Nutr 2011;31:65–87.
[10] White JA, Guo YD, Baetz K, Beckett-Jones B, Bonasoro J, Hsu KE, et al. Identification of the retinoic acid-inducible all-trans-retinoic acid 4-hydroxylase. J Biol Chem 1996;271:29922–7.
[11] Thatcher JE, Isoherranen N. The role of CYP26 enzymes in retinoic acid clearance. Expert Opin Drug Metab Toxicol 2009;5:875–86.
[12] Thatcher JE, Buttrick B, Shaffer SA, Shimshoni JA, Goodlett DR, Nelson WL, et al. Substrate specificity and ligand interactions of CYP26A1, the human liver retinoic acid hydroxylase. Mol Pharmacol 2011;80:228–39.
[13] Lutz JD, Dixit V, Yeung CK, Dickmann LJ, Zelter A, Thatcher JE, et al. Expression and functional characterization of cytochrome P450 26A1, a retinoic acid hydroxylase. Biochem Pharmacol 2009;77:258–68.
[14] Chithalen JV, Luu L, Petkovich M, Jones G. HPLC-MS/MS analysis of the products generated from all-trans-retinoic acid using recombinant human CYP26A. J Lipid Res 2002;43:1133–42.
[15] White JA, Ramshaw H, Taimi M, Stangle W, Zhang A, Everingham S, et al. Identification of the human cytochrome P450, P450RAI-2, which is predominantly expressed in the adult cerebellum and is responsible for all-trans-retinoic acid metabolism. Proc Natl Acad Sci USA 2000;97:6403–8.
[16] Taimi M, Helvig C, Wisniewski J, Ramshaw H, White J, Amad M, et al. A novel human cytochrome P450, CYP26C1, involved in metabolism of 9-cis and all-trans isomers of retinoic acid. J Biol Chem 2004;279:77–85.
[17] Idres N, Marill J, Flexor MA, Chabot GG. Activation of retinoic acid receptor-dependent transcription by all-trans-retinoic acid metabolites and isomers. J Biol Chem 2002;277:31491–8.
[18] Abu-Abed S, MacLean G, Fraulob V, Chambon P, Petkovich M, Dolle P. Differential expression of the retinoic acid-metabolizing enzymes CYP26A1 and CYP26B1 during murine organogenesis. Mech Dev 2002;110:173–7.
[19] MacLean G, Abu-Abed S, Dolle P, Tahayato A, Chambon P, Petkovich M. Cloning of a novel retinoic-acid metabolizing cytochrome P450, Cyp26B1, and comparative expression analysis with Cyp26A1 during early murine development. Mech Dev 2001;107:195–201.
[20] Abu-Abed S, Dolle P, Metzger D, Beckett B, Chambon P, Petkovich M. The retinoic acid-metabolizing enzyme, CYP26A1, is essential for normal hindbrain patterning, vertebral identity, and development of posterior structures. Genes Dev 2001;15:226–40.
[21] Yashiro K, Zhao X, Uehara M, Yamashita K, Nishijima M, Nishino J, et al. Regulation of retinoic acid distribution is required for proximodistal patterning and outgrowth of the developing mouse limb. Dev Cell 2004;6:411–22.
[22] Uehara M, Yashiro K, Mamiya S, Nishino J, Chambon P, Dolle P, et al. CYP26A1 and CYP26C1 cooperatively regulate anterior–posterior patterning of the developing brain and the production of migratory cranial neural crest cells in the mouse. Dev Biol 2007;302:399–411.
[23] Tay S, Dickmann L, Dixit V, Isoherranen N. A comparison of the roles of peroxisome proliferator-activated receptor and retinoic acid receptor on CYP26 regulation. Mol Pharmacol 2010;77:218–27.
[24] Xi J, Yang Z. Expression of RALDHs (ALDH1As) and CYP26s in human tissues and during the neural differentiation of P19 embryonal carcinoma stem cell. Gene Expr Patterns 2008;8:438–42.
[25] Thatcher JE, Zelter A, Isoherranen N. The relative importance of CYP26A1 in hepatic clearance of all-trans retinoic acid. Biochem Pharmacol 2010;80:903–12.
[26] Fiorella PD, Napoli JL. Microsomal retinoic acid metabolism. Effects of cellular retinoic acid-binding protein (type I) and C18-hydroxylation as an initial step. J Biol Chem 1994;269:10538–44.
[27] Samokyszyn VM, Gall WE, Zawada G, Freyaldenhoven MA, Chen G, Mackenzie PI, et al. 4-hydroxyretinoic acid, a novel substrate for human liver microsomal UDP-glucuronosyltransferase(s) and recombinant UGT2B7. J Biol Chem 2000;275:6908–14.

[28] Shen AL, Porter TD, Wilson TE, Kasper CB. Structural analysis of the FMN binding domain of NADPH-cytochrome P-450 oxidoreductase by site-directed mutagenesis. J Biol Chem 1989;264:7584–9.
[29] Rosenberger M, Neukom C. Retinoic acid metabolite. 3. Total synthesis of (2E,4E,6E,8E)-3,7-dimethyl-9-[6,6-dimethyl-2-(hydroxymethyl)-1-cyclohexen-1-yl]-2,4,6,8-nonatetraenoic acid. J Org Chem 1982;47:1782–5.
[30] Kawanobe T, Kogami K, Hayashi K, Matsui M. New synthesis of γ-homocyclogeranial, γ-dihydroionone and their derivatives. Agric Biol Chem 1984;48:461–4.
[31] Kumar A, Singh D, Mahale GD, Rana RK, Kharade M. Process for preparation of highly pure isotretinoin. US Patent 7,763,748, July 27, 2010.
[32] Omura T, Sato R. The carbon monoxide-binding pigment of liver microsomes. I. Evidence for its hemoprotein nature. J Biol Chem 1964;239:2370–8.
[33] Yamamoto Y, Zolfaghari R, Ross AC. Regulation of CYP26 (cytochrome P450RAI) mRNA expression and retinoic acid metabolism by retinoids and dietary vitamin A in liver of mice and rats. FASEB J 2000;14:2119–27.
[34] Fujii H, Sato T, Kaneko S, Gotoh O, Fujii-Kuriyama Y, Osawa K, et al. Metabolic inactivation of retinoic acid by a novel P450 differentially expressed in developing mouse embryos. EMBO J 1997;16:4163–73.
[35] Sakai Y, Meno C, Fujii H, Nishino J, Shiratori H, Saijoh Y, et al. The retinoic acid-inactivating enzyme CYP26 is essential for establishing an uneven distribution of retinoic acid along the anterio-posterior axis within the mouse embryo. Genes Dev 2001;15:213–25.
[36] Alder A, Bigler P, Werck-Reichhart D, Al-Babili S. In vitro characterization of synechocystis CYP120A1 revealed the first nonanimal retinoic acid hydroxylase. FEBS J 2009;276:5416–31.
[37] Rosenberger M, Neukom C. Retinoic acid metabolites. 2. Total synthesis of rac-(2E,4E,6E,8E)-3,7-dimethyl-9-(6-carboxy-2,6-dimethyl-3-oxo-1-cyclohexen-1-yl)-2,4,6,8-nonatetraenoic acid and rac-(2E,4E,6E,8E)-3,7-dimethyl-9-[2,6-dimethyl-6-(hydroxymethyl)-3-oxo-1-cyclohexen-1-yl)-2,4,6,8-nonatetraenoic acid. J Org Chem 1982;47:1779–82.
[38] Fiorella PD, Napoli JL. Expression of cellular retinoic acid binding protein (CRABP) in *Escherichia coli*. Characterization and evidence that holo-CRABP is a substrate in retinoic acid metabolism. J Biol Chem 1991;266:16572–9.
[39] Roberts AB, Lamb LC, Sporn MB. Metabolism of all-trans-retinoic acid in hamster liver microsomes: oxidation of 4-hydroxy- to 4-keto-retinoic acid. Arch Biochem Biophys 1980;199:374–83.
[40] Satre MA, Penner JD, Kochhar DM. Pharmacokinetic assessment of teratologically effective concentrations of an endogenous retinoic acid metabolite. Teratology 1989;39:341–8.
[41] Totah RA, Rettie AE. Cytochrome P450 2C8: substrates, inhibitors, pharmacogenetics, and clinical relevance. Clin Pharmacol Ther 2005;77:341–52.
[42] Karlsson MSA, Sirsjo A, Eriksson LA. Homology models and molecular modeling of human retinoic acid metabolizing enzymes cytochrome P450 26A1 (CYP26A1) and P450 26B1 (CYP26B1). J Chem Theory Comput 2008;4:1021–7.